International Journal of Innovative
Computing, Information and Control
Volume **14**, Number **3**, June **2018**

ICIC International ©2018 ISSN 1349-4198
pp. **847–860**

DESIGN OF A NON-THERMAL FOOD PROCESSING SYSTEM UTILIZING WIRE DISCHARGE OF DUAL ELECTRODES IN UNDERWATER

Kei Eguchi[1], Anurak Jaiwanglok[2], Amphawan Julsereewong[2]
Farzin Asadi[3], Hiroto Abe[1] and Ichirou Oota[4]

[1]Department of Information Electronics
Fukuoka Institute of Technology
3-30-1 Wajirohigashi, Higashi-ku, Fukuoka 811-0295, Japan
eguti@fit.ac.jp

[2]Faculty of Engineering
King Mongkut's Institute of Technology Ladkrabang
1 Soi Chalongkrung 1, Ladkrabang, Bangkok 10520, Thailand
anurak.jai@hotmail.com; amphawan.ju@kmitl.ac.th

[3]Mechatronics Engineering Department
Kocaeli University
Umuttepe Yerleşkesi 41380, Kocaeli, Turkey
farzin.asadi@kocaeli.edu.tr

[4]Department of Electronics Engineering and Computer Science
National Institute of Technology, Kumamoto College
2659-2 Suya, Koushi-shi, Kumamoto 861-1102, Japan
oota-i@kumamoto-nct.ac.jp

Received October 2017; revised February 2018

Abstract. *To provide nutritious and fresh processed foods, non-thermal food processing technologies have been developed in recent years. Among others, a non-thermal food processing method utilizing underwater shockwaves has cost-effectiveness. In this method, the design of a high voltage multiplier and its discharging method are key factors for processing target foods effectively. This paper proposes a non-thermal food processing system utilizing wire discharge of dual electrodes in underwater. Unlike conventional non-thermal food processing systems, the proposed system has two pairs of electrodes with thin metal wires. Owing to the electric discharge using thin metal wires, the energy to generate underwater shockwaves can be decreased. For this reason, by only one electric discharge, both sides of the target food are crushed by the proposed technique. The experiments using a laboratory prototype clarified that the proposed method can soften the whole flesh of the target food effectively. Furthermore, by assuming a four-terminal model, an equivalent model of the high voltage multiplier was analyzed theoretically. Concerning the series-connected voltage multiplier, the design conditions were derived to estimate the characteristics such as output voltage and power efficiency.*
Keywords: Discharge, Multiple electrodes, Non-thermal food processing, Underwater shockwaves, High electric discharge, High voltage multipliers

1. **Introduction.** A food processing technology without heating [1] can provide nutritious and fresh processed foods, because the destruction of nutrients is not caused with an increase in temperature. For this reason, in order to support the healthy life of people, the non-thermal food processing is receiving much attention in recent years. In past studies, many non-thermal food processing technologies [1], for example, High Hydrostatic Pressure (HHP), High Voltage Arc Discharge (HVAD), and Cold Plasma (CP), have been

proposed. Among others, a non-thermal processing utilizing underwater shockwaves [2,3] is one of the most promising technologies, because it can provide nutritious and fresh processed foods at low cost. In this method, first, a high voltage such as 3.5kV is generated by high voltage multipliers. The output voltage of the high voltage multiplier is stored in a big capacitor. Then, electrical energy stored in the big capacitor is discharged in a pressure vessel filled with water, where the electrical energy turns into shockwave energy. Finally, underwater shockwaves destroy a target food. In this food processing, only the internal tissue of the target food is disrupted by internal destruction which is called spalling destruction. For this reason, the high voltage multiplier and the pressure vessel are key components for processing the target food effectively. However, the development of the pressure vessel has been studied deeply in past studies [4-6]. For example, Miyafuji et al. and Iyama et al. developed the pressure vessel for manufacturing rice powder in 2011 [4] and 2016 [5]. Higa et al. clarified the characteristics of the shock wave propagation by computer simulation [6]. Hence, we concentrated on the design of a high voltage multiplier and its discharging method in this paper.

In the non-thermal processing utilizing underwater shock-waves, the Cockcroft-Walton Voltage Multiplier (CWVM) [7] has been used to generate a high voltage. Unlike a transformer with high turn ratio, the CWVM has advantages in the point of cost and weight. However, the output voltage of the traditional CWVM decreases according to the increase of the number of stages. To develop efficient CWVMs, various challenges have been tackled in past studies. For example, a cascade CWVM was proposed by Wang and Luerkens in 2013 [8]. The cascade CWVM [8] can reduce the voltage ripple magnitude by employing symmetrical structure. However, a transformer with center-tapped secondary is necessary. The transformer-less voltage multiplier was suggested by Young et al. and Razzak et al. in 2011 [9] and 2015 [10]. By connecting a boost converter with a CWVM, the voltage multipliers in [9,10] offers a high voltage. Following these studies, by combining a multilevel boost converter with a CWVM, a high voltage multiplier was designed by Bhaskar et al. in 2016 [11]. However, a large inductor is required to achieve high step-up conversion.

To reduce the voltage drop caused by the increase of the number of stages, a bipolar CWVM was developed by Iqbal and Besar and Eguchi et al. in 2007 [12] and 2011 [13]. By combining the outputs of positive and negative multipliers, the bipolar CWVM can generate a high stepped-up voltage. Following this study, a hybrid symmetrical CWVM was proposed by Iqbal in 2014 [14]. In this voltage multiplier, the voltage drop is improved by the hybrid symmetrical bipolar topology. However, the response speed is slow, because diode switches are driven by AC voltages supplied by a commercial power source.

To solve this problem, an inductor-less high-speed CWVM [15,16] was proposed by Eguchi et al. and Abe et al. in 2014 and 2015, and a split-source voltage multiplier was developed by Katzir and Shmilovitz in 2016 [17]. In [15,16], in order to drive the CWVM at high speed, high-speed rectangular pulses are generated by using a full waveform rectifier and high/low side drivers. On the other hand, by combining a full waveform rectifier and transformers, Katzir's CWVM achieves high speed. However, in order to achieve high gain, transformers are used in [17]. Following this study, our research team designed a high voltage multiplier without full waveform rectifiers [18,19]. In [18], AC-AC converters are employed instead of the full waveform rectifier. By connecting the bipolar CWVM with AC-AC converters, a high gain is achieved with small number of stages. However, the response speed is still slow though not only high gain but also simple circuit configuration can be realized by [18]. On the other hand, the high voltage multiplier of [19] is composed of plural CWVMs. By connecting plural CWVMs via level shift drivers, not only high response speed but also high gain are achieved by [19]. However, due to

complexity of the circuit configuration, the circuit characteristics, such as output voltage and power efficiency, are not clear theoretically. For this reason, in order to clarify the characteristics, we analyze the high voltage multiplier of [19] theoretically. Furthermore, in the point of discharging method, conventional non-thermal food processing systems using the above-mentioned voltage multipliers have the following drawbacks: 1) the conventional system requires high energy to generate an underwater shockwave and 2) the conventional system is difficult to process the whole flesh of the target food by only one electric discharge, because it has only one pair of electrodes [20]. Of course, the whole flesh of the target food can be processed by setting plural pairs of electrodes [21]. However, the conventional method needs at least two high voltage relays. For this reason, the conventional discharging method is disadvantageous in point of hardware cost and processing time.

In this paper, we develop a non-thermal food processing system utilizing wire discharge of dual electrodes. Unlike conventional systems, the proposed system has two pairs of electrodes with thin metal wires. Owing to the thin metal wires, the energy to generate an underwater shockwave can be decreased. Therefore, by only one electric discharge, the whole flesh of the target food can be softened by the proposed system. Furthermore, in order to estimate the characteristics of the proposed voltage multiplier, a four-terminal equivalent model is derived theoretically. The theoretical analysis gives simple formulas about the output voltage and power efficiency. To demonstrate the effectiveness of the proposed system, experimental evaluation is performed concerning the laboratory prototype.

The contributions of this work are as follows: 1) by using a four-terminal equivalent model, we clarified the characteristics of the high voltage multiplier of [19] theoretically and 2) by utilizing wire discharge of dual electrodes, we realized effective non-thermal food processing by only one electric discharge.

The rest of this paper is organized as follows. Section 2 describes the configuration of the proposed non-thermal food processing system in order to clarify the idea of this work. Section 3 explains the circuit configuration of the proposed high voltage multiplier and gives the theoretical formulas to estimate the characteristics of the proposed voltage multiplier. Section 4 demonstrates the effectiveness of the proposed non-thermal food processing system through laboratory experiments. Finally, Section 5 discusses conclusion and future work of this study.

2. **System Configuration.**

The architecture of the proposed non-thermal food processing system is illustrated in Figure 1. As Figure 1 shows, the non-thermal food processing system mainly consists of a high voltage multiplier, a big capacitor, a high voltage switch, and a pressure vessel. By utilizing an underwater shockwave, the system of Figure 1 can process a target food without heating. However, in the conventional system shown in Figure 1(a) [20], it is difficult to process the whole flesh of the target food by only one electric discharge, because the conventional system has only one pair of electrodes. Thus, the softened part of the target food depends on the position of the electrodes. Of course, the whole flesh of the target food can be processed by the non-thermal food processing system with plural pairs of electrodes [21]. However, this method increases hardware cost and processing time. Unlike the conventional system of Figure 1(a), the proposed system of Figure 1(b) has two pairs of electrodes with thin metal wires. Owing to the thin metal wires, we can decrease the energy for generating an underwater shockwave. Therefore, by only one electric discharge, the wire discharge of dual electrodes achieves the non-thermal processing from the both sides of the target food. The operation principle of the proposed system is as follows.

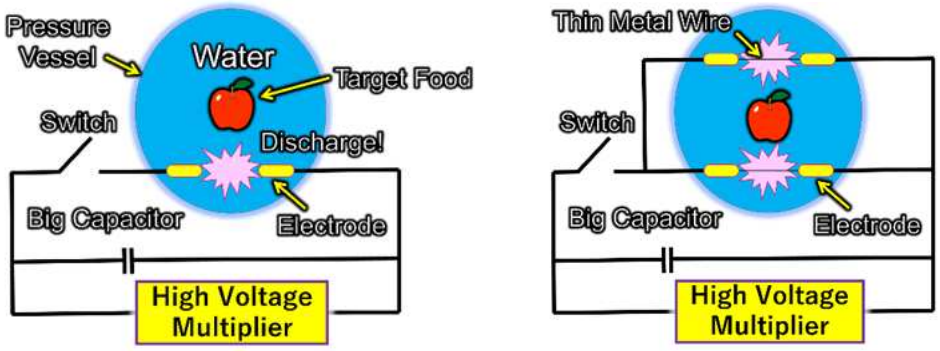

(a) (b)

FIGURE 1. Laboratory prototype of the proposed non-thermal food processing system: (a) conventional system [20] and (b) proposed system

First, the high voltage multiplier generates a high stepped-up voltage, such as 3.5kV, from an AC input 100@60Hz. The output voltage of the high voltage multiplier is stored in a big capacitor with 200μF capacity. Next, by turning on the high voltage switch, the electric charge stored in the big capacitor is discharged from two electrodes at the same time. By utilizing wire discharge of dual electrodes, underwater shockwaves are generated in the pressure vessel. Owing to the thin metal wires between electrodes, the proposed method can decrease the energy necessary to generate an underwater shockwave. Then, the water around electrodes evaporates instantaneously by the electric discharge. After that, a shockwave occurs by implosion. Finally, unlike the conventional method, the underwater shockwaves destroy the target food from both sides, where the target food is crushed by internal destruction.

In the following section, the characteristics of the high voltage multiplier used in the proposed system will be analyzed theoretically.

3. High Voltage Multiplier.

3.1. Circuit configuration.

Figure 2 illustrates the circuit configuration of our voltage multiplier proposed in [19]. The proposed voltage multiplier generates the following output voltage:

$$V_{out} = V_{po} - V_{mo}, \tag{1}$$

where

$$V_{po} \cong (4M_p + 1) \cdot V_{cw},\ V_{mo} \cong -(4M_m + 1) \cdot V_{cw},\ \text{and}\ V_{cw} = 2N \cdot (V_{in} - V_{th})$$

In (1), V_{in} is an AC input value, V_{th} is a threshold voltage of the diode switch, N $(= 1, 2, \ldots)$ is the number of stages of the positive/negative multiplier in the first multiplier block, M_p $(= 1, 2, \ldots)$ is the number of stages of the positive multiplier in the second multiplier block, M_m $(= 1, 2, \ldots)$ is the number of stages of the negative multiplier in the second multiplier block, V_{po} is the positive output voltage, V_{mo} is the negative output voltage, and V_{cw} is the output voltage of the first multiplier block. As you can see from (1), the proposed voltage multiplier can provide more than 3.5kV output under conditions that $N = 1$, $M_p = 2$, and $M_m = 1$. In previous works, it is known that a 3.5kV output is necessary to destroy fruits such as apples, and tomato. To generate more than 3.5kV output, the traditional CWVM requires 28 times step-up gain. Therefore, the number of stages of the traditional CWVM is 14. On the other hand, the maximum number of

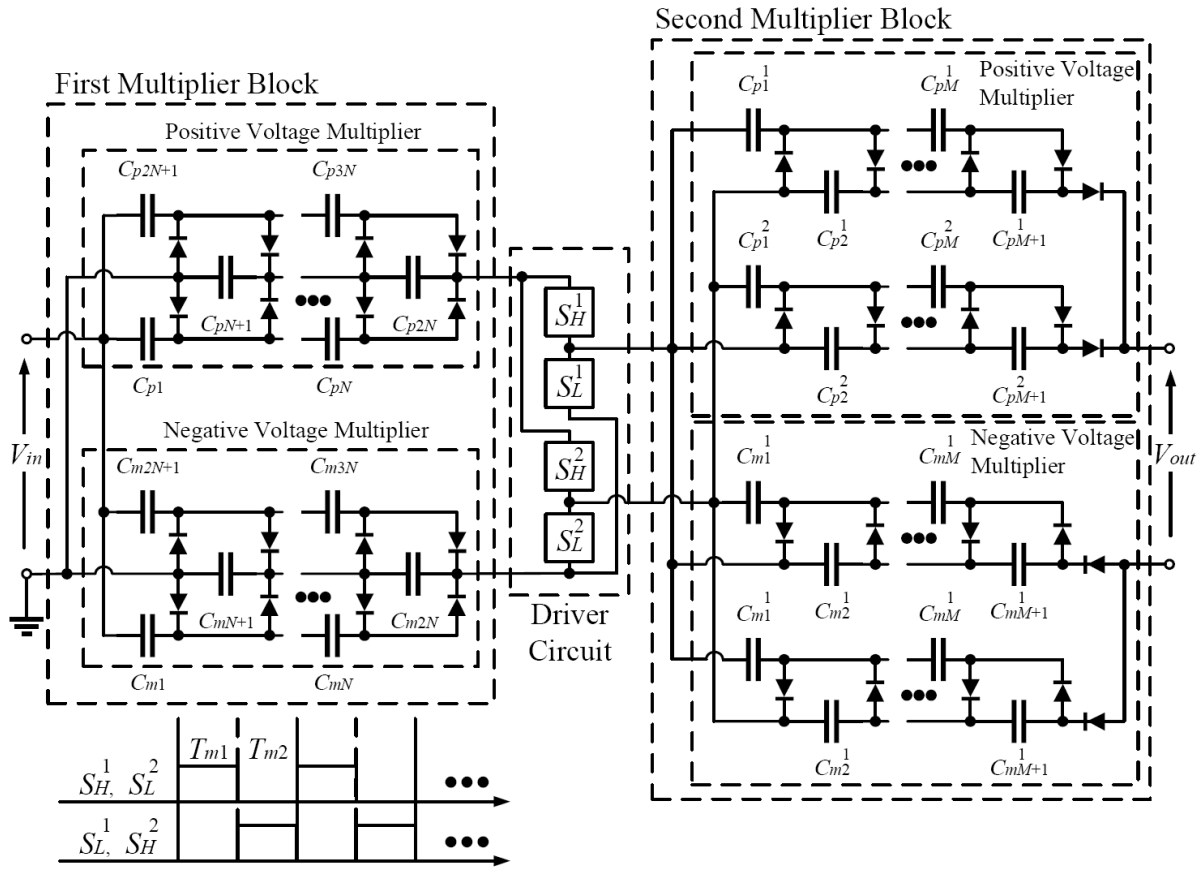

FIGURE 2. High voltage multiplier using level shift drivers [19]

TABLE 1. Comparison of the number of circuit components

Number of components	Traditional Cockcroft-Walton voltage multiplier ($N = 13$)	Proposed voltage multiplier ($N = 1$, $M_p = 2$ and $M_m = 1$)
Diode	26	24
Capacitor	26	18
Transistor	0	4
Total	52	46

stages in the proposed voltage multiplier is 3. Therefore, the proposed voltage multiplier of Figure 2 can achieve higher response speed than the traditional CWVM.

Table 1 demonstrates the comparison of the number of circuit components between the proposed voltage multiplier and the traditional Cockcroft-Walton voltage multiplier. As Table 1 shows, the number of circuit components of the proposed voltage multiplier is smaller than that of the traditional CWVM. The operation of the proposed voltage multiplier is as follows. First, the AC input 100@60Hz is converted to the DC voltage by the first multiplier blocks. Then, by utilizing the DC output of the first multiplier block, high speed rectangular pulses are generated by the driver circuit. Finally, by amplifying the outputs of the driver circuit, the second multiplier block generates the positive and negative high stepped-up voltages. The plus/minus terminals of the big capacitor are connected to the outputs V_{po}/V_{mo}, respectively.

3.2. **Theoretical analysis.** In order to clarify the characteristics of the high voltage multiplier shown in Figure 2, the power efficiency and output voltage are derived by assuming the four-terminal equivalent circuit [22-24]. The four-terminal equivalent circuit is depicted in Figure 3. The four-terminal equivalent circuit consists of an ideal transformer with $1 : m$ ratio and an internal resistor R_{SC}. The four-terminal equivalent circuit of the high voltage multiplier is derived under conditions that 1) the step-up gain is 28 ($N = 1$, $M_p = 2$ and $M_m = 1$), 2) the input is a rectangular waveform, and 3) the period of the rectangular waveform is much smaller than time constant.

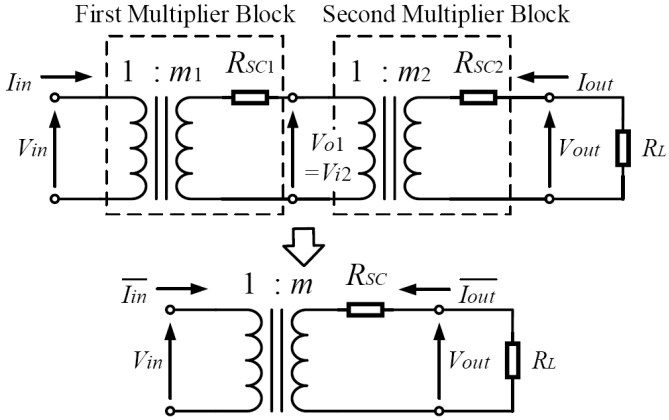

FIGURE 3. Four-terminal equivalent model of the proposed voltage multiplier

In this theoretical analysis, we obtain the four four-terminal equivalent circuit of the high voltage multiplier by using the instantaneous equivalent circuits shown in Figure 4, where Figure 4 denotes the instantaneous equivalent circuits in a steady state. The parameters in Figure 4 are as follows: R_{on} is the on-resistance of the transistor switch, R_d is the on-resistance of the diode, and V_{th} is the threshold voltage of the diode.

In the first multiplier block shown in Figures 4(a) and 4(b), the differential value of the electric charge in C_{pj} and C_{mj} $(j = 1, \ldots, 3)$ satisfies

$$\sum_{i=1}^{2} \Delta q_{T_{ri}}^{pj} = 0 \text{ and } \sum_{i=1}^{2} \Delta q_{T_{ri}}^{mj} = 0, \tag{2}$$

where

$$T_r = \sum_{i=1}^{2} T_{ri} \text{ and } T_{r1} = T_{r2} = \frac{T_r}{2}.$$

In (2), $\Delta q_{T_{ri}}^{pj}$ denotes the differential value of the j-th capacitor of the positive voltage multiplier and $\Delta q_{T_{ri}}^{mj}$ denotes the differential value of the j-th capacitor of the negative voltage multiplier. Here, the interval T_r is determined by the frequency of the AC input V_{in}.

In Figures 4(a) and 4(b), the following conditions are satisfied:

$$\Delta q_{T_{ri}}^{p1} = \Delta q_{T_{ri}}^{p3} \text{ and } \Delta q_{T_{ri}}^{m1} = \Delta q_{T_{ri}}^{m3}, \tag{3}$$

because Figure 4 has a symmetrical structure. While the state is T_{ri}, we have the differential values of electric charges in the input and output terminals, $\Delta q_{T_{r1},V_i^1}$, $\Delta q_{T_{r2},V_i^1}$, $\Delta q_{T_{r1},V_{po}^1}$, $\Delta q_{T_{r2},V_{po}^1}$, $\Delta q_{T_{r1},V_{mo}^1}$, and $\Delta q_{T_{r2},V_{mo}^1}$ as follows:

State-T_{r1}:

$$\begin{aligned}&\Delta q_{T_{r1},V_i^1} = -\Delta q_{T_{r1}}^{p1} - \Delta q_{T_{r1}}^{p3} + \Delta q_{T_{r1}}^{m1} + \Delta q_{T_{r1}}^{m3},\\ &\Delta q_{T_{r1},V_{po}^1} = \Delta q_{T_{r1}}^{p1} + \Delta q_{T_{r1}}^{p2} + \Delta q_{T_{r1}}^{p3} \text{ and } \Delta q_{T_{r1},V_{mo}^1} = -\Delta q_{T_{r1}}^{m2}.\end{aligned} \tag{4}$$

State-T_{r2}:

$$\begin{aligned}&\Delta q_{T_{r2},V_i^1} = \Delta q_{T_{r2}}^{p1} + \Delta q_{T_{r2}}^{p3} - \Delta q_{T_{r2}}^{m1} - \Delta q_{T_{r2}}^{m3},\ \Delta q_{T_{r2},V_{po}^1} = \Delta q_{T_{r2}}^{p2}\\ &\text{and } \Delta q_{T_{r2},V_{mo}^1} = -\Delta q_{T_{r2}}^{m1} - \Delta q_{T_{r2}}^{m2} - \Delta q_{T_{r2}}^{m3}.\end{aligned} \tag{5}$$

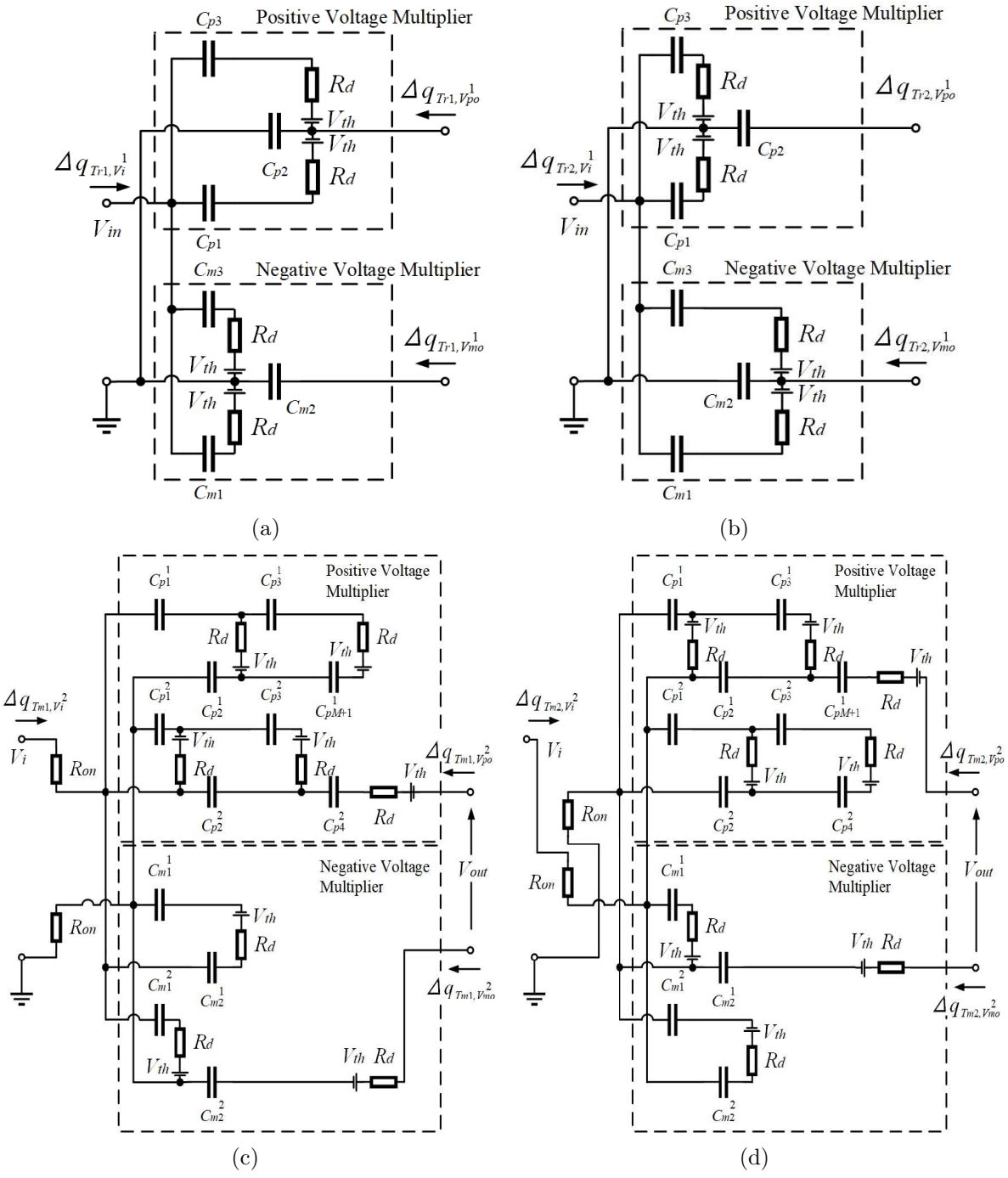

FIGURE 4. Instantaneous equivalent circuits in a steady state: (a) State-T_{r1}, (b) State-T_{r2}, (c) State-T_{m1}, and (d) State-T_{m2}

In (4) and (5), the following equation is satisfied:

$$\Delta q_{V_{po}^1} = -\Delta q_{V_{mo}^1}, \tag{6}$$

because the output terminals V_{po} and V_{mo} are connected via the output load. Here, using the Kirchhoff's current laws, the input and output current are expressed as

$$\overline{I_{in}} = \frac{1}{T}\left(\sum_{i=1}^{2} \Delta q_{T_i,V_{in}}\right) = \frac{\Delta q_{V_{in}}}{T} \text{ and } \overline{I_{out}} = \frac{1}{T}\left(\sum_{i=1}^{2} \Delta q_{T_i,V_{out}}\right) = \frac{\Delta q_{V_{out}}}{T}, \tag{7}$$

because the overall change of the input and output currents is zero in the steady state. In (7), $\Delta q_{V_{in}}$ and $\Delta q_{V_{out}}$ are electric charges in V_{in} and V_{out}, respectively. Therefore, we get the relation between the input current and the output current by substituting (2)-(6) into (7) as follows:

$$\overline{I_i^1} = -4\overline{I_o^1}, \tag{8}$$

where

$$\overline{I_o^1} = \overline{I_{po}^1} = -\overline{I_{mo}^1}.$$

From (8), the parameter $m1$ in Figure 3 is derived as $m1 = 4$.

Next, the consumed energy in one period is discussed to derive the SC resistance R_{SC1} of the first multiplier block. As Figures 4(a) and 4(b) show, the instantaneous equivalent circuits of the first multiplier block have the same structure. In other words, the consumed energy in Figures 4(a) and 4(b) is the same. Therefore, the consumed energy W_{T_r} of the first multiplier block can be expressed as

$$W_{T_r} = \sum_{i=1}^{2} W_{T_{ri}} = \frac{4R_d}{T_r}\left(\Delta q_{V_{po}^1}\right)^2. \tag{9}$$

In (9), dielectric loss is not considered, because the input is assumed as a rectangular pulse. In Figure 3, the consumed energy W_T of the four-terminal equivalent circuit is given by

$$W_T = R_{SC} \cdot \frac{(\Delta q_{V_{out}})^2}{T}. \tag{10}$$

Therefore, from (9) and (10), we have the SC-resistance of the first multiplier blocks, R_{SC1}, as

$$R_{SC1} = 4R_d. \tag{11}$$

On the other hand, as shown in Figures 4(c) and 4(d), the second multiplier blocks also have two states: State-T_{m1} and State-T_{m2}. In a steady state, the differential value of the electric charge in C_{pk}^1, C_{pk}^2, C_{ml}^1, and C_{ml}^2 ($(k = 1, \ldots, 4)$ and $(l = 1, 2)$) satisfies

$$\sum_{i=1}^{2} \Delta q_{T_{mi}}^{1pk} = 0,\ \sum_{i=1}^{2} \Delta q_{T_{mi}}^{2pk} = 0,\ \sum_{i=1}^{2} \Delta q_{T_{mi}}^{1ml} = 0 \text{ and } \sum_{i=1}^{2} \Delta q_{T_{mi}}^{2ml} = 0, \tag{12}$$

where

$$T_m = \sum_{i=1}^{2} T_{mi} \text{ and } T_{m1} = T_{m2} = \frac{T_m}{2}.$$

In (12), $\Delta q T_{mi}^{1pk}$ and $\Delta q T_{mi}^{2pk}$ denote the differential value of the k-th capacitor of the upper positive voltage multiplier and the lower positive voltage multiplier, respectively. On the other hand, $\Delta q T_{mi}^{1ml}$ and $\Delta q T_{mi}^{2ml}$ denote the differential value of the l-th capacitor of the upper negative voltage multiplier and the lower negative voltage multiplier, respectively. Here, the interval T_m is determined by the switching frequency of the driver circuit (see in Figure 2).

In the second multiplier blocks, the following equations are satisfied:

$$\Delta q_{T_{m1}}^{1pk} = \Delta q_{T_{m2}}^{2pk},\ \Delta q_{T_{m1}}^{2pk} = \Delta q_{T_{m2}}^{1pk},\ \Delta q_{T_{m1}}^{1ml} = \Delta q_{T_{m2}}^{2ml},\ \text{and}\ \Delta q_{T_{m1}}^{2ml} = \Delta q_{T_{m2}}^{1ml}, \tag{13}$$

because each voltage multiplier has a parallel-connected structure with opposite polarity. While the state is T_{mi}, we have the differential values of electric charges in the input and output terminals, $\Delta q_{T_{m1},V_i^2}$, $\Delta q_{T_{m2},V_i^2}$, $\Delta q_{T_{m1},V_{po}^2}$, $\Delta q_{T_{m2},V_{po}^2}$, $\Delta q_{T_{m1},V_{mo}^2}$, and $\Delta q_{T_{m2},V_{mo}^2}$ as follows:

State-T_{m1}:

$$\begin{aligned} &\Delta q_{T_{m1},V_i^2} = -\Delta q_{T_{m1}}^{1p1} + \Delta q_{T_{m1}}^{2p1} - \Delta q_{T_{m1}}^{2p2} - \Delta q_{T_{m1}}^{2p3} + \Delta q_{T_{m1}}^{1m2} + \Delta q_{T_{m1}}^{2m1}, \\ &\Delta q_{T_{m1},V_{po}^2} = \Delta q_{T_{m1}}^{2p4} \text{ and } \Delta q_{T_{m1},V_{mo}^2} = -\Delta q_{T_{m1}}^{2m2}. \end{aligned} \tag{14}$$

State-T_{m2}:

$$\begin{aligned} &\Delta q_{T_{m2},V_i^2} = \Delta q_{T_{m2}}^{1p1} - \Delta q_{T_{m2}}^{1p2} - \Delta q_{T_{m2}}^{1p3} - \Delta q_{T_{m2}}^{2p1} + \Delta q_{T_{m2}}^{1m1} + \Delta q_{T_{m2}}^{2m2}, \\ &\Delta q_{T_{m2},V_{po}^2} = \Delta q_{T_{m2}}^{1p4} \text{ and } \Delta q_{T_{m2},V_{mo}^2} = -\Delta q_{T_{m2}}^{1m2}. \end{aligned} \tag{15}$$

In (14) and (15), the following equation is satisfied

$$\Delta q_{V_{po}^2} = -\Delta q_{V_{mo}^2}, \tag{16}$$

because the output terminals V_{po} and V_{mo} are connected via an output load. Here, by substituting (12)-(16) into (7), we have the relation between the input current and the output current as follows:

$$\overline{I_i^2} = -7\overline{I_{out}}, \tag{17}$$

where

$$\overline{I_{out}} = \overline{I_{po}^2} = -\overline{I_{mo}^2}.$$

From (17), the parameter $m2$ in Figure 3 is derived as $m2 = 7$.

Next, the consumed energy in one period is discussed to derive the SC resistance R_{SC2} of the second multiplier block. As Figures 4(c) and 4(d) show, energy is consumed by R_d and R_{on}. The consumed energy W_{T_m} of the second multiplier blocks can be expressed as

$$W_{T_m} = \sum_{i=1}^{2} W_{T_{mi}} = \frac{8R_d + 98R_{on}}{T_m} \left(\Delta q_{V_{po}^2}\right)^2, \tag{18}$$

because the instantaneous equivalent circuits have the same structure in State-T_{m1} and State-T_{m2}. Therefore, from (10) and (18), we have the SC-resistance of the second multiplier blocks, R_{SC2}, as

$$R_{SC2} = 8R_d + 98R_{on}. \tag{19}$$

Finally, by combining (11) and (19), the parameters m and R_{SC} of the proposed voltage multiplier are obtained as

$$m = 28 \text{ and } R_{SC} = 204R_d + 98R_{on}. \tag{20}$$

In other words, we have the equivalent circuit of the proposed voltage multiplier as follows:

$$\begin{bmatrix} \overline{V_{in}} \\ \overline{I_{in}} \end{bmatrix} = \begin{bmatrix} 1/28 & 0 \\ 0 & 28 \end{bmatrix} \begin{bmatrix} 1 & 204R_d + 98R_{on} \\ 0 & 1 \end{bmatrix} \begin{bmatrix} \overline{V_{out}} \\ -\overline{I_{out}} \end{bmatrix}. \tag{21}$$

Therefore, from (21), the power efficiency and output voltage are derived as follows:

$$\eta = \frac{R_L}{R_L + (204R_d + 98R_{on})} \times \left(1 - \frac{9V_{th}}{7V_{in}}\right) \tag{22}$$

and

$$V_{out} = \frac{28R_L}{R_L + (204R_d + 98R_{on})} \times \left(V_{in} - \frac{9}{7}V_{th}\right). \tag{23}$$

Form (22) and (23), we can estimate the characteristics of the high voltage multiplier easily.

4. Experiment.

4.1. **Experimental setup.** To confirm the validity of the proposed non-thermal food processing system, we conducted experiments concerning the laboratory prototype shown in Figure 5. The experimental circuit of Figure 5 was built with a high voltage multiplier, a high voltage relay, and a big capacitor. Figure 6 shows the high voltage multiplier realizing 28 × gain. The proposed voltage multiplier of Figure 6 was implemented with commercially available components shown in Table 2. In the experiments, the input voltage is 100V@60Hz. From Figure 6, more than 4kV output is offered to the big capacitor shown in Figure 7. The capacity of Figure 7 is 200μF and the rated voltage is 4000VDC. Figure 7 is a custom-made capacitor which is composed of polypropylene film and insulating oil. To control the connection between the high voltage multiplier and the big capacitor, the high voltage relay shown in Figure 8 is used as the high voltage switch shown in Figure 1(b). In Figure 8, the HV contact is 12kV and insulation to ground is 20kV. The terminals of the big capacitor are connected to the electrodes in the chamber shown in Figure 9. In the experiments, in order to investigate the discharging process of the non-thermal food processing, we used the 60 × 30 × 36cm acrylic water tank shown in Figure 9. As you can see from Figures 9(b) and 9(c), thin metal wires were set between electrodes in order to generate shockwaves at low energy. To investigate the effect of non-thermal food processing, the wrapped apple was used as a target food. Of course, the water-rich food can be processed easily by small energy. However, by the color change of the apple flesh, we can confirm the effect of the non-thermal food processing.

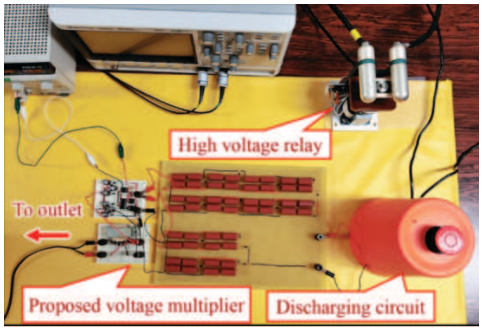

FIGURE 5. Laboratory prototype

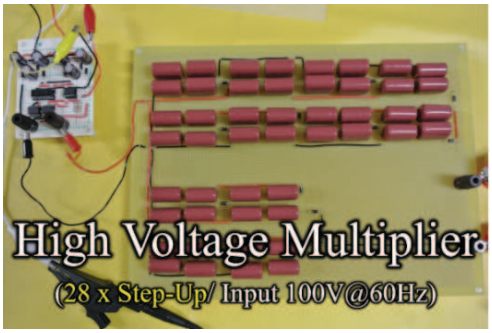

FIGURE 6. High voltage multiplier

TABLE 2. Circuit components of the high voltage multiplier

Block Name	Component	Model/Value
AC-DC rectifier	Capacitor	33μF
	Diode	1N4007
Driver circuit	Switch	AQW216
	Driver IC	TD62004APG
	2-Phase clock generator	PIC12F1822
Bipolar voltage multiplier	Capacitor	1μF
	Diode	1N4007
	Output capacitor	2.2μF

FIGURE 7. Big capacitor

FIGURE 8. High voltage relay

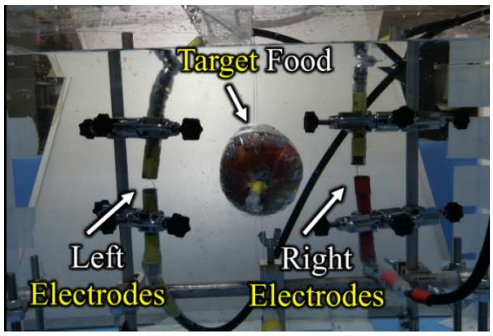

(a)

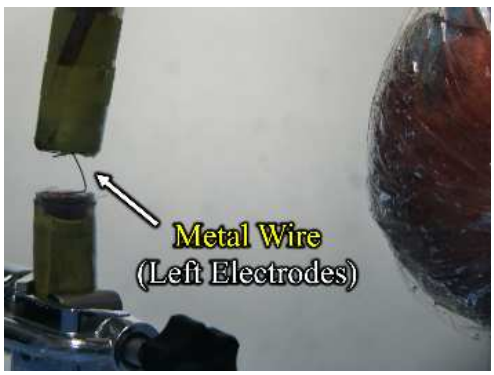

(b)

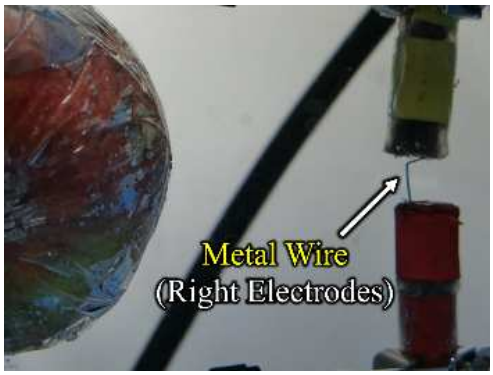

(c)

FIGURE 9. Acrylic water tank: (a) overview, (b) left electrodes and (c) right electrodes

4.2. **Experimental results.** Figure 10 demonstrates the discharging phenomenon captured by the high speed camera EX-100PRO, where the gap between copper electrodes was set to 10mm. As Figure 10 shows, the high-voltage electric discharge occurred from both electrodes at the same time. In other words, both sides of the target food are destroyed by only one electric discharge.

Figure 11 demonstrates the cross-section of the processed food. In the result of the conventional method [20] shown in Figure 11(a), the whole flesh of the target food cannot be crushed by only one electric discharge. Therefore, to process the whole flesh of the target food, the conventional method needs at least two high voltage relays [21]. Otherwise, higher energy must be stored in the output capacitor. In other words, in order to process the whole flesh of the target food, the conventional method [20] requires the higher output voltage and the bigger output capacitor than the proposed method.

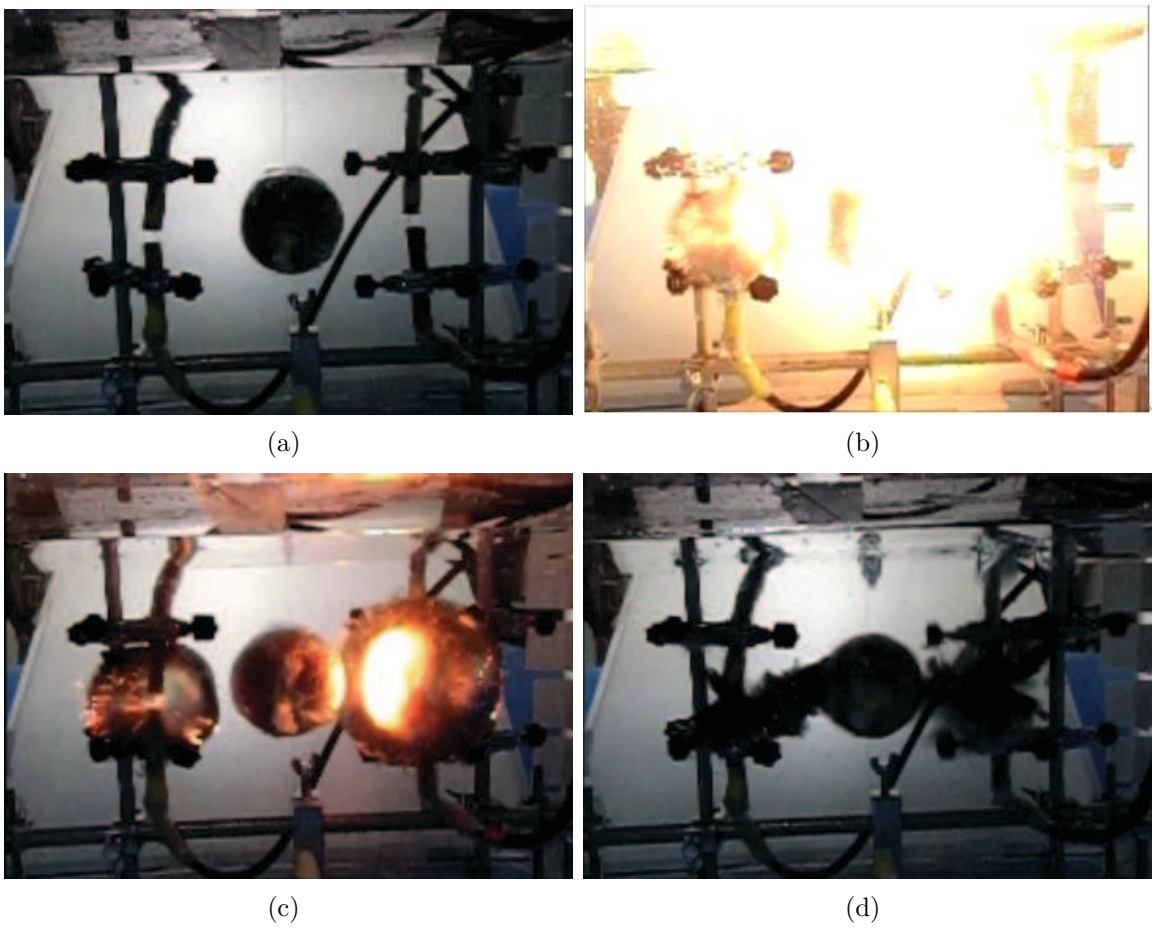

(a) (b)

(c) (d)

FIGURE 10. Discharging phenomenon: (a) State-1, (b) State-2, (c) State-3, and (d) State-4

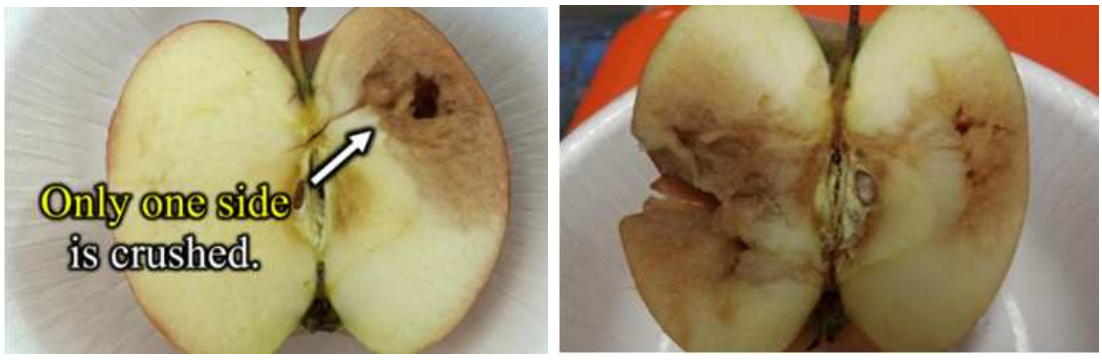

(a) (b)

FIGURE 11. Cross-section of the processed food: (a) conventional method and (b) proposed method

On the other hand, unlike the conventional result of Figure 11(a), the proposed method can soften the whole flesh of the target food by only one electric discharge as shown in Figure 11(b). In Figure 11(b), the hardness of the target food was changed from about 54.5N to 35.4N by the proposed method. Of course, the proposed non-thermal food processing system can completely crush the target food by increasing the number of electric discharge.

5. **Conclusions.** In this paper, we have designed a high voltage non-thermal food processing system utilizing wire discharge of dual electrodes. The results of this study are as follows.

First, the properties of the proposed high voltage multiplier were analyzed theoretically. By assuming a four-terminal equivalent model, simple formulas to obtain power efficiency and output voltage were derived. The derived formulas will help users to estimate the characteristics of the proposed voltage multiplier.

Then, the effectiveness of the proposed non-thermal food processing system was confirmed by the experiments using a laboratory prototype. By utilizing wire discharge of dual electrodes, the whole flesh of the target food was softened by the proposed method. Concretely, the hardness of the target food was changed from about 54.5N to 35.4N by only one electric discharge.

In a future study, we are going to investigate the contamination of water caused by the melting of metal wires and copper electrodes.

Acknowledgment. This research was financially supported by the Urakami Foundation for Food and Food Culture Promotion. The authors also gratefully acknowledge the helpful comments and suggestions of the reviewers, which have improved the presentation.

REFERENCES

[1] M. Stoica, L. Mihalcea, D. Bprda and P. Alexe, Non-thermal novel food processing technologies – An overview, *Journal of Agroalimentary Processes and Technologies*, vol.19, no.2, pp.212-217, 2013.

[2] C. H. Zhang, T. Namihira, T. Kiyan, K. Nakashima, S. Katsuki, H. Akiyama, H. Ito and Y. Imaizumi, Investigation of shockwave produced by large volume pulsed discharge under water, *IEEE Pulsed Power Conf.*, pp.1377-1380, 2005.

[3] S. Shinzato, Y. Higa, T. Tamaki, H. Iyama and S. Itoh, Computational simulation of underwater shock wave propagation using smoothed particle hydrodynamics, *Materials Science Forum*, vol.767, pp.86-91, 2013.

[4] Y. Miyafuji, K. Shimojima, S. Tanaka, K. Naha, T. Aka, H. Maehara and S. Itoh, Development of the pressure vessel for manufacturing the rice-powder using the underwater shock wave, *Proc. of the ASME 2011 Pressure Vessels and Piping Conf.*, pp.53-56, 2011.

[5] H. Iyama, M. Nishi, Y. Higa, K. Shimojima, O. Higa and S. Itoh, Numerical simulation on manufacturing of pressure vessel for shock food processing using explosive forming, *Proc. of the ASME 2016 Pressure Vessels and Piping Conf.*, 2016.

[6] Y. Higa, K. Shimojima, H. Iyama, O. Higa, A. Takemoto, S. Itoh and A. Yasuda, Computational simulation for evaluation of food softening treatment vessel using underwater shockwave, *Proc. of the ASME 2016 Pressure Vessels and Piping Conf.*, 2016.

[7] A. Lamantia, P. Maranesi and L. Radrizzani, The dynamics of the Cockcroft-Walton voltage multiplier, *Proc. of the IEEE Power Electronics Specialists Conf.*, pp.485-490, 1990.

[8] J. Wang and P. Luerkens, Complete model of parasitic capacitances in a cascade voltage multiplier in the high voltage generator, *Proc. of the IEEE ECCE Asia Downunder*, pp.18-24, 2013.

[9] C. H. Young, C. C. Ko, M. H. Chen and C. C. Wu, A Cockcroft-Walton voltage multiplier with PFC using ZC-ZVT auxiliary circuit, *Proc. of the IECON 2011*, pp.1001-1005, 2011.

[10] M. A. Razzak, S. Chakraborty and Z. Tasneem, Design of a multistage 0.1/12 kV DC-DC matrix converter using Cockcroft-Walton voltage multiplier topology, *Proc. of the 2015 IEEE International WIE Conference on Electrical and Computer Engineering*, pp.309-312, 2015.

[11] M. S. Bhaskar, S. Padmanaban, F. Blaabjerg, L. E. Norum and A. H. Ertas, 4Nx non-isolated and non-inverting hybrid interleaved multilevel boost converter based on VLSIm cell and Cockcroft Walton voltage multiplier for renewable energy applications, *Proc. of the 2016 IEEE International Conference on Power Electronics, Drives and Energy Systems*, pp.1-6, 2016.

[12] S. Iqbal and R. Besar, A bipolar Cockcroft-Walton voltage multiplier for gas lasers, *American Journal of Applied Sciences*, vol.4, no.10, pp.795-801, 2007.

[13] K. Eguchi, I. Oota, S. Terada and H. Zhu, 2x/3x step-up switched-capacitor (SC) AC-DC converters for RFID tags, *International Journal of Intelligent Engineering and Systems*, vol.4, no.1, pp.1-9, 2011.

[14] S. Iqbal, A hybrid symmetrical voltage multiplier, *IEEE Trans. Power Electronics*, vol.29, no.1, pp.6-12, 2014.
[15] K. Eguchi, S. Pongswatd, S. Terada and I. Oota, Parallel-connected high voltage multiplier with symmetrical structure, *Applied Mechanics and Materials*, vol.619, pp.173-177, 2014.
[16] K. Abe, H. Sasaki, I. Oota and K. Eguchi, Improvement of an output voltage efficiency of a high voltage generator for non-thermal food processing systems, *ICIC Express Letters*, vol.9, no.11, pp.3087-3092, 2015.
[17] L. Katzir and D. Shmilovitz, Effect of the capacitance distribution on the output impedance of the half-wave Cockcroft-Walton voltage multiplier, *Proc. of the 2016 IEEE Applied Power Electronics Conference and Exposition*, pp.3655-3658, 2016.
[18] K. Eguchi, A. Wongjan, A. Julsereewong, W. Do and I. Oota, Design of a high-voltage multiplier combined with Cockcroft-Walton voltage multipliers and switched-capacitor AC-AC converters, *International Journal of Innovative Computing, Information and Control*, vol.13, no.3, pp.1007-1019, 2017.
[19] K. Abe, I. Oota, W. Do and K. Eguchi, Synthesis of a high step-up bipolar voltage multiplier using level shift drivers, *Proc. of 2016 the 6th International Workshop on Computer Science and Engineering*, pp.305-309, 2016.
[20] K. Abe, R. Ogata, K. Eguchi, K. Smerpitak and S. Pongswatd, Study on non-thermal food processing utilizing an underwater shockwave, *Indian Journal of Science and Technology*, vol.10, no.4, pp.1-5, 2017.
[21] K. Eguchi, K. Abe, R. Ogata and I. Oota, Experimental study of a non-thermal food processing system using a series-connected bipolar voltage multiplier with multiple electrodes, *Proc. of the 5th IIAE International Conference on Industrial Application Engineering*, pp.214-219, 2017.
[22] K. Eguchi, T. Sugimura, S. Pongswatd, K. Tirasesth and H. Sasaki, Design of a multiple-input parallel SC DC-DC converter and its efficiency estimation method, *ICIC Express Letters*, vol.3, no.3(A), pp.531-536, 2009.
[23] K. Eguchi, K. Fujimoto and H. Sasaki, A hybrid input charge-pump using micropower thermoelectric generators, *IEEJ Trans. Electrical and Electronic Engineering*, vol.7, no.4, pp.415-422, 2012.
[24] K. Tsubomi, S. Terada, K. Eguchi and I. Oota, Improvement and analysis of equivalent circuit for switching converter by considering electric power loss, *The Trans. of IEICE C*, vol.97-C, no.10, pp.365-375, 2014.